



# Fluorinated graphene suspension for flexible and printed electronics: Flakes, 2D films, and heterostructures

Irina V. Antonova<sup>a,b,c,\*</sup>, Irina I. Kurkina<sup>d</sup>, Anton K. Gutakovskii<sup>a,b</sup>, Igor A. Kotin<sup>a</sup>, Artem I. Ivanov<sup>a</sup>, Nadezhda A. Nebogatikova<sup>a,b</sup>, Regina A. Soots<sup>a</sup>, Svetlana A. Smaglova<sup>d</sup>

<sup>a</sup> Rzhanov Institute of Semiconductor Physics SB RAS, Novosibirsk 630090, Lavrentiev av. 13, Russia

<sup>b</sup> Novosibirsk State University, 630090, Pirogov str. 2, Novosibirsk, Russia

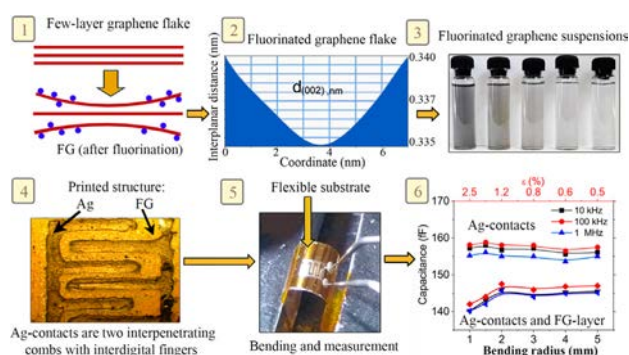
<sup>c</sup> Novosibirsk State Technical University, 630073, K. Marx str. 20, Novosibirsk, Russia

<sup>d</sup> Ammosov North-Eastern Federal University, 677000, Belinskii str. 58, Yakutsk, Russia

## HIGHLIGHTS

- Excellent mechanical properties for the fluorinated graphene films with different fluorination degree are demonstrated.
- FG films possess a unique combination of properties for 2D dielectric films including the transparency.
- Fluorinated graphene suspension is suggested for the dielectric films, especially for flexible and printed electronics.

## GRAPHICAL ABSTRACT



## ARTICLE INFO

### Article history:

Received 31 October 2018

Received in revised form 27 November 2018

Accepted 28 November 2018

Available online 27 December 2018

### Keywords:

Fluorinated graphene

HREM

Heterostructures

2D printing techniques

FG flexibility

## ABSTRACT

Fluorinated graphene (FG), the most stable derivative of graphene, is suggested for the role of functional material (weak fluorination degree) and the dielectric layers for graphene and other 2D materials, especially for flexible and printed electronics. The main findings discussed in the present study are (1) an excellent mechanical properties of FG in bending conditions for the first time measured for FG with different fluorination degree; (2) the 97–99% transparency of FG films with thickness up to 25 nm in wide range of wavelengths, (3) a ultralow leakage current and a high breakdown field in the printed cross-bar structures; (4) a smooth increase in interplanar spacing by 1–2% from the center of few-layered fluorinated graphene flakes to their edges; (5) observation of only C—C related G line without defect related D line in Raman spectra in the case of giant amplification of Raman scattering for FG films printed at Ag layers. Unchanged characteristics of fluorinated graphene films up to stretching-strain values of 2.5–4% were demonstrated. Generally, it can be stated that fluorinated graphene films have great promise in flexible and printed electronics.

© 2018 Published by Elsevier Ltd. This is an open access article under the CC BY-NC-ND license (<http://creativecommons.org/licenses/by-nc-nd/4.0/>).

## 1. Introduction

For the development of graphene-based electronics, dielectric layers capable of providing a high-quality interface of this material with adjacent materials are required. Indeed, transport in graphene proceeds at

\* Corresponding author at: Rzhanov Institute of Semiconductor Physics SB RAS, Novosibirsk 630090, Lavrentiev av. 13, Russia.

E-mail address: [antonova@isp.nsc.ru](mailto:antonova@isp.nsc.ru) (I.V. Antonova).

heterointerfaces with adjacent layers. It is a well-known fact that, due to the structure of hexagonal boron nitride being close to that of graphene, a good graphene/h-BN interface forms ensuring a high charge-carrier mobility in graphene up to 80,000 cm<sup>2</sup>/Vs (or to 140,000 cm<sup>2</sup>/Vs in the case of h-BN/graphene/h-BN structures) at room temperature [1–4]. To boron nitride problems, the lack of a technology for obtaining large-area h-BN layers of a desired quality can be classed, whereas the drawbacks of the material proper include its mechanical properties remaining unchanged on the decrease of its thickness from several monolayers down to one monolayer, a relatively strong interaction between the layers and, hence, the restrictions in obtaining thin layers and in using the material in flexible electronics [5,6]. An alternative material for flexible electronics, as expected, is a fluorinated graphene.

Fluorinated graphene, an up-rising member of the graphene family, combines a two-dimensional layer structure, wide bandgap a high stability, and it attracts significant attention because of its unique nanostructure and carbon-fluorine bonds [7–9]. The rapidly development of graphene chemistry has been observed for the last few years resulting in a wide portfolio of graphene derivatives including a wide spectrum of fluorination approaches [10,11]. The fluorination process can be realised by an exposure to fluorine-containing gases (XeF<sub>2</sub>, F<sub>2</sub>) (for instance, [12,13]), with the use of plasma (for instance, [14]), or by exfoliation of fluorographite (for instance, [15]). Fluorination of graphene oxide (GO) can be achieved by the hydrothermal or solvothermal fluorination using hydrofluoric acid, BF<sub>3</sub>-etherate and other fluorine-containing reagents [16–18]. The graphene suspension fluorination enables a facile and scalable access to the applications. Fluorinated graphene films obtained by different methods presently become widely used in interface engineering [19], for the improvement of FET characteristics [20,21], for a wide spectrum of biological and medical applications [22] and, in the case of weakly fluorinated graphene suspensions, for modification of electrodes in lithium-ion batteries [23,24]. An attractive feature in the development of device structures with the use of fluorinated graphene is based on a relatively high stability of FG, in comparison with graphene oxide or hydrogenated graphene (the C–F bond energy is above 100 kcal/mol [25], defluorination point ~450 °C [26]).

A cheap, simple, and scalable method for obtaining fluorinated graphene based on treating graphene in aqueous solutions of hydrofluoric acid (HF) was proposed [27,28]. That method can be used for the fluorination of large-area polycrystalline graphene and graphene suspensions. Thus, fluorinated graphene films can be easily created from graphene suspensions and used for 2D printing technologies. Moreover, in view of the additional splitting and fragmentation of graphene flakes during the fluorination process [28] very smooth films are created from this suspension of fluorinated graphene. As its demonstrated below, it leads to a relatively low fluorination degree (<50%). Nevertheless, transparent and insulating films can be obtained from this suspension. It was shown that a weakly fluorinated suspension can be used for creating self-organized quantum-dot arrays in a fluorinated graphene matrix [29]. In this case, one can create layers with current-voltage characteristics exhibiting the phenomenon of negative differential resistance, make it possible to control currents in the film, and observe resistive switchings in films with quantum dots [30]. The considerable potential in using films obtained from fluorinated graphene suspensions calls for detailed studies of the structural properties of this material aimed at revealing the way the fluorination process proceeds and the properties the obtained material possesses.

In the present study, the properties of the fluorinated graphene suspension, crossbar structures with a FG layer and the structures with two interpenetrating combs created by means of the 2D printing technique on a flexible substrate are considered. The possibility to observe the phenomenon of giant Raman scattering in the case in which the fluorinated graphene layer was applied onto the printed layer of Ag contacts was shown. Attractive characteristics of FG as an insulating layer for thicknesses ranging from 20 to 40 nm were demonstrated. For the

first time, data gained while studying the properties of fluorinated graphene films on flexible substrates with various fluorination degrees (capacitance and/or conductivity) on their deformations (bending) are reported. Stability of parameters and potential in using fluorinated graphene for flexible electronics up to stretching strains of 2.5–4% were found.

## 2. Experimental section

### 2.1. Preparation of graphene and fluorinated graphene suspensions

An important starting step in the preparation of fluorinated graphene suspensions is the synthesis of the graphene suspension. We used the electrochemical exfoliation of high-oriented pyrolytic graphite (HOPG) with its additional processing with ultrasound. The electrolyte, in which the cleavage occurred, was an acid solution (NH<sub>4</sub>)<sub>2</sub>S<sub>2</sub>O<sub>8</sub> of 0.15 g per 100 mL of water. As a result of the electrochemical exfoliation, a non-oxidized graphene suspension with a flake thickness of 3–10 nm was obtained [31]. An alternative exfoliation method that was also used in the present study was the liquid exfoliation of natural graphite combined with ultrasonic processing and centrifugation. Then, filtration of suspension into components with various flake size was performed. By means of filtration on track membranes, flakes with lateral sizes exceeding 1.2 μm (suspension A), flakes sized 0.4–1.2 μm (suspension B) and flakes smaller than 0.4 μm (suspension C) were isolated. The track membranes have their pore sizes of 1.2 mm and 0.4 mm and one or two filtration steps allow us to separate the suspension with different lateral sizes. Flakes with lateral sizes smaller than 400 nm were then used for 2D printing of FG layers. The latter value is about ~50 times smaller than the printer nozzle diameter.

As it was shown in publication [26–28], the suspension fluorination process proceeds in a weak (~3–7%) solution of hydrofluoric acid. The elucidation for the chosen fluorination conditions in detail is given in Ref. [27, 28] and the references within these papers. In contrast to the alternative variant for fluorination of the oxide graphene suspension developed in Ref. [16, 32] only the graphene suspension was used for the fluorination and the conditions for the fluorination process without oxidation were found. For testing, the films from the FG suspension are created on Si or other desirable substrates by means of drops, with the same volume (0.1 mL), or 2D printing. The maximum fluorination degree of graphene flakes is ~40–50% and the fluorination time was varied depending on the lateral sizes of graphene flakes and their thickness. During the fluorination process due to additional exfoliation, the thickness of fluorinated graphene flakes strongly decreases down to 1–5 monolayers. After fluorination of suspension, the remainder of the hydrofluoric acid was removed from the solution by displacement on water. As a result, a water-based FG suspension, suitable and ready for use as FG ink for 2D printing was obtained.

### 2.2. Printing and characterization methods

The films and the structures were fabricated by the 2D printing method. A Dimatix FUJIFILM DMP-2831 printer equipped with a DMC-11610 printing head with 16 nozzle carriers of about 20-μm diameter was used for printing. The printing process was implemented on both solid and flexible substrates. As flexible substrates, Polyethyleneterephthalate (PET) substrates with an adhesive coating (Lamond), Epson-paper substrates for jet printing, and polyamide films (Kapton) were used. We used 50- and 200-μm thick films. The thickness of different substrates was checked by means of a micrometer. During the printing process, the substrate temperature was maintained at 60 °C.

A Solver PRO NT-MDT scanning microscope was used for obtaining atomic force microscopy (AFM) images of suspension flakes and film surfaces, and for determining the film thicknesses. The measurements were conducted in both contact and semi-contact mode. Silicon cantilever tips

(HA\_C/Au) with a typical resonance frequency of 19 and 37 kHz, a force constant of 0.26 and 0.65 N/m, respectively, and a tip radius <10 nm were used. Differentiation of regions according to their chemical composition was based on images recorded in lateral-force (friction-force) mode. Raman spectra were recorded at room temperature, the excitation wavelength is 514.5 nm (2.41-eV argon ion laser). In order to avoid the heating of samples with laser radiation, the laser beam power was decreased to 2–3 mW. Scanning electron microscopy (SEM) images were obtained using a JEOL JSM-7800F scanning electron microscope with the energy of primary electrons equal to 2 keV. JEOL JSM 7800F was equipped with a super-hybrid objective lens and the “Gentle Beam” system, which allows obtaining high-resolution images at low accelerating voltages. The use of such systems makes it possible to obtain images of the films without the deposition of electrically conductive coatings. Film-structure features were studied by means of high-resolution transmission electron microscopy (HRTEM) using JEOL-4000EX microscope operated at 400-kV energy. This microscope is characterized by a point-to-point resolution of 0.16 nm. For the HRTEM study, the graphene suspension was applied dropwise onto thin (10 nm) carbon films and then dried for several hours. Digital processing of HRTEM images was performed by means of the DIGITAL MICROGRAPH software (GATAN) and specialized GPA scripts. The sheet resistance of obtained films was studied using the four-probe Jandel equipment and HM21 Test Unit at room temperature. Measured X-ray photoelectron spectroscopy (XPS) spectra permitted the study of the chemical composition of obtained films. The XPS measurements were carried out with a K-Alpha (Thermo Scientific) spectrometer equipped with a monochromatized Al K $\alpha$  X-ray source (1486.68 eV). The spectra were acquired at 90° take-off angle in the constant analyzer energy mode with a pass energy of 100 eV (0.5 eV step) and 20 eV (0.05 eV step) for survey and high-resolution region scans, respectively. For poorly conductive samples a dual-beam charge compensation system (flood gun) was used to

minimize surface charging. The base pressure in the analysis chamber was  $7 \times 10^{-10}$  mbar and during sample analysis with the flood gun on it was the range of  $(1-3) \times 10^{-7}$  mbar.

The transmission spectra were recorded using an SF-56 spectrometer (wavelength ~ 300–1000 nm) and Bruker IFS-113V Fourier transform spectrometer (wavelength ~ 2–20  $\mu$ m) in a two-beam scheme (channel with sample and reference channel).

Capacitance-voltage (C-V) and current-voltage (I-V) characteristics of fabricated structures were measured using a precision LCR meter E4980AL and a Keithley picoammeter (model 6485) at room temperature. Moreover, cyclic deformations with simultaneously testing the electrical parameters of the material or structures were carried out. Home-made installations for applying tensile and compressive strain to the tested films were used.

### 3. Results and discussion

#### 3.1. Functional and insulated FG suspension and films

From graphene suspensions obtained by electrochemical exfoliation of high-oriented pyrolytic graphite (HOPG) and an additional processing of the obtained mixture of graphite particles with ultrasound, by means of filtration by track membranes, particles with lateral sizes >1.2  $\mu$ m (suspension A), particles sized 0.4–1.2  $\mu$ m (suspension B) and <0.4  $\mu$ m (suspension C) were extracted. The initial graphene suspension and the B-series suspensions after fluorination treatments held during different times are shown in Fig. 1(a,b). The increase in the fluorination time leads to an enhanced transparency of the suspension due to the growth of fluorination degree. Moreover, as it was mentioned above (experimental section), fluorination leads to a strong decrease in the flake lateral size and thickness. The higher the fluorination degree, the smaller the flake size and thickness [28]. The AFM and SEM images of

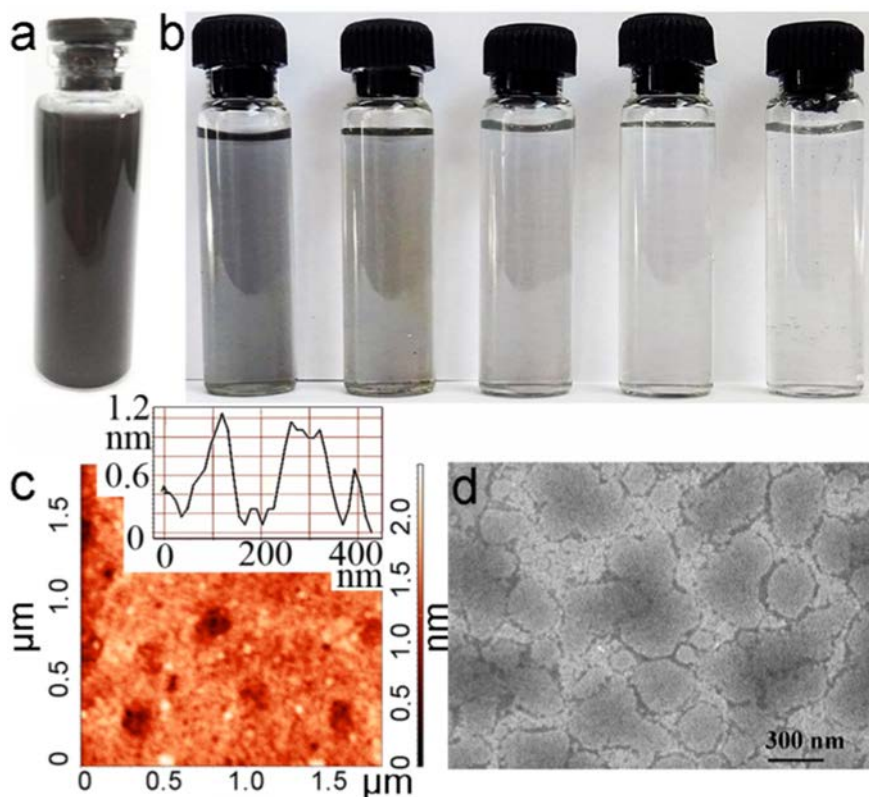


**Fig. 1.** (a) Initial graphene suspension of type B (pristine flakes had lateral sizes 1.2–0.4  $\mu$ m) with composition ~1 mg/mL and (b) the same suspension B fluorinated in a 6-% solution of hydrofluoric acid in water during 3, 5, 7, 9, and 11 days (from left to right). (c) AFM and (d) SEM images of an FG film (suspension B) on a silicon substrate after fluorination during 6 days. Insert in (c) gives the profile cross the three separate flakes.

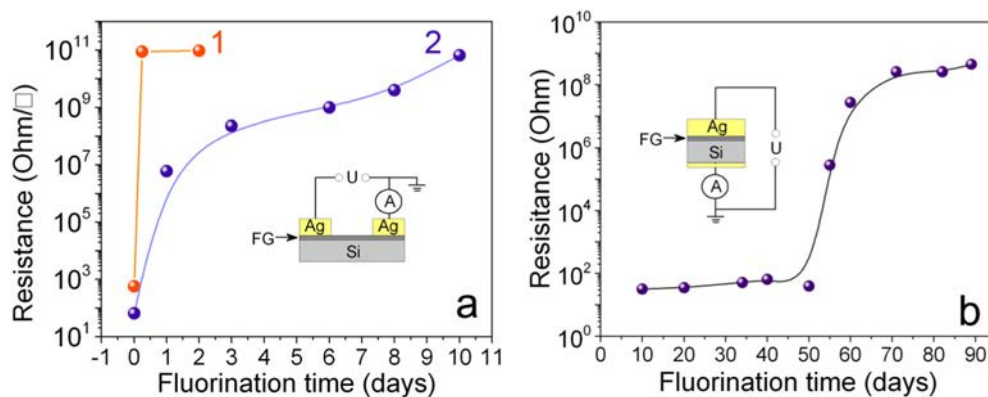


**Fig. 2.** Resistances of the films obtained from suspensions fluorinated in an aqueous solution of hydrofluoric acid measured in lateral (a) and vertical (b) configurations. The curves correspond to different suspensions used for fluorination: (a) 1 – suspension C formed by flakes with lateral sizes  $<0.4 \mu\text{m}$ , 2 – the flakes with sizes  $0.4\text{--}1.2 \mu\text{m}$  (suspension B), and (b) the flakes with lateral sizes  $>1.2 \mu\text{m}$  (suspension A). In the case (b), the area of the contacts was  $0.3 \text{ mm}^2$ . The thickness of the films determined with use of AFM was varied in the range of  $70\text{--}20 \text{ nm}$  (increase in the fluorination degree leads to a decrease in the FG thickness).

the films created from the 6-day fluorinated suspension B are given in Fig. 1(c,d). The vertical scale of AFM image and the profile cross of the three separate flakes demonstrate the FG film relief. The roughness calculated from few AFM images with the size  $2\text{--}3 \mu\text{m}$  was equal to  $0.3\text{--}0.5 \text{ nm}$ .

Fig. 2 shows the resistance of the FG films deposited onto Si substrates from suspensions with different sizes of the initial graphene flakes (suspensions A, B, and C) as a function of the time of sample treatment in the aqueous solution of hydrofluoric acid. The films were created by means of suspension drops with the same volume on the Si substrate. It is necessary to note that the increase in the fluorination degree (increase in the flake hydrophilicity) is combined with the additional fragmentation of the flakes (flakes become thinner and smaller) [28]. As a result of a complex change in the suspension properties, the drop spreading on Si surface is enlarged. This fact leads to a decrease in the FG film thickness. For instance, the thickness of the films presented in Fig. 2(b) varied with time from  $70$  to  $20 \text{ nm}$ . The strong increase in the resistance corresponds to the creation of weakly fluorinated graphene first (functional material with graphene quantum dots), and then to the transfer from the conductive to insulated state. It is seen that a decrease in the flake size of initial graphene suspension leads to an abrupt decreasing of required fluorination time. The latter is related to the properties of nanosize graphene flakes, making possible a chemical behavior not observed in larger flakes. More specifically, fine and, hence, thin flakes experience deformation that allows the reaction with fluorine which forbidden in undeformed graphene [33].

A transition into the non-conducting state is observed at fluorination degrees above  $\sim 23\%$  [21]. In what follows, we will denote fluorinated graphene suspensions and non-conducting films based on such suspensions as FG, whereas for films with a lower fluorination degree (incomplete fluorination) we introduce the abbreviation WFG (weakly fluorinated graphene). As it was mentioned previously, graphene quantum dots form in the latter case. Those quantum dots present nanocrystals, embedded in a fluorinated graphene matrix, in which the recharging of size quantization levels was observed [27,29].

### 3.2. Structural properties of fluorinated graphene

Fig. 3 shows XPS spectra for films obtained from suspensions with different fluorination degrees (fluorine-to-carbon atomic ratio). Attention should be drawn to the fact that only peaks due to C-CF ( $284.5 \text{ eV}$ ), C-CF ( $285.6 \text{ eV}$ ), and CF ( $288.3 \text{ eV}$ ) bonds are observed in XPS spectra in the vicinity of the peak C1s. Peaks with a higher content of fluorine  $\text{CF}_x$  with  $x > 1$  (such as  $\text{CF}_2$  or  $\text{CF}_3$ ) normally observed at other fluorination methods [7,34,35] in our case were never observed. The fluorination degree was determined in two ways, from the ratio of the

areas under the F1s and C1s peaks ( $284.5 \text{ eV}$ ) in the XPS spectra or, alternatively, by the formula  $x_{\text{tot}} = S_{\text{C-F}} / (S_{\text{C}} + S_{\text{C-F}} + S_{\text{C-F}})$ , where S are the areas under the peaks obtained by decomposition of the spectrum in the vicinity of C1s into components. The mean of the obtained values was adopted as the fluorination-degree value of the given film. It was found that, on increasing the fluorination time, the degree of fluorination, as a rule, never exceeds  $40\text{--}50\%$ . Fig. 1(c,d) show AFM and SEM images of a film prepared from a suspension with fluorination degree  $\sim 35\%$  on Si substrate. A transition into the non-conducting state is commonly observed at fluorination degrees above  $\sim 21\%$  [21].

Repeated measurements of XPS spectra for fluorinated graphene films as well as measurements of film resistivity clearly demonstrate the stability of its properties with a time. It is necessary to note, that the water-based fluorinated graphene suspension demonstrates some weak defluorination in a time scale  $\sim 1\text{--}2$  months (decrease in pH of solution). Moreover, the transmission of suspension and insulated properties of film are not degraded with a time.

In some cases, the defluorination process was observed for fluorinated graphene. For example, graphene fluorination by means of exposure in  $\text{XeF}_2$  gas leads to a high fluorine content (spectra with the dominance of  $\text{CF}_2$  and  $\text{CF}_3$  peaks) and it declines (fixed by XPS measurements) over several days before stabilizing [13]. It was found that, namely, the magnitude of the  $\text{CF}_2$  and  $\text{CF}_3$  peaks was decreased in time. Other researchers demonstrate the stability of fluorinated graphene created by the same method [12] and monitored by high-resolution electron energy loss spectroscopy for the loss of the C-F-related peak under annealing in vacuum. The intensity of peak attributed to the C—F bonds was found to be unchanged up to  $300 \text{ }^\circ\text{C}$ . In the last case, the XPS spectra did not contain  $\text{CF}_2$ - and  $\text{CF}_3$ -related peaks. The stability of the lateral graphene/fluorinated graphene heterostructures is also demonstrated in Ref. [34]. In the case of fluorinated graphene flakes, the C—F bonds created at the edge or other defects are especially stable. Another variant of the FG instability is observed for the samples immersed in solvents, including deionized water, isopropanol, acetone, dichloromethane and chloroform for a time at room temperature [36]. These films also have very intensive  $\text{CF}_2$  and  $\text{CF}_3$  components, and these components, again, decline first. In our case, some defluorination occurs in water, but the suspension for insulated films maintains this property.

Fig. 4 shows Raman spectra for films of different fluorination degrees. The amplitudes of the G peak due to the C—C bonds ( $1590 \text{ cm}^{-1}$ ), the D peak due to defects ( $1390 \text{ cm}^{-1}$ ), and the second-harmonics 2D peak ( $2700 \text{ cm}^{-1}$ ) all decrease with the growth of fluorination degree. The latter occurs at all fluorination methods and is related with the appearance of the bandgap in fluorinated graphene. It was found that in the case in which a fluorinated graphene suspension

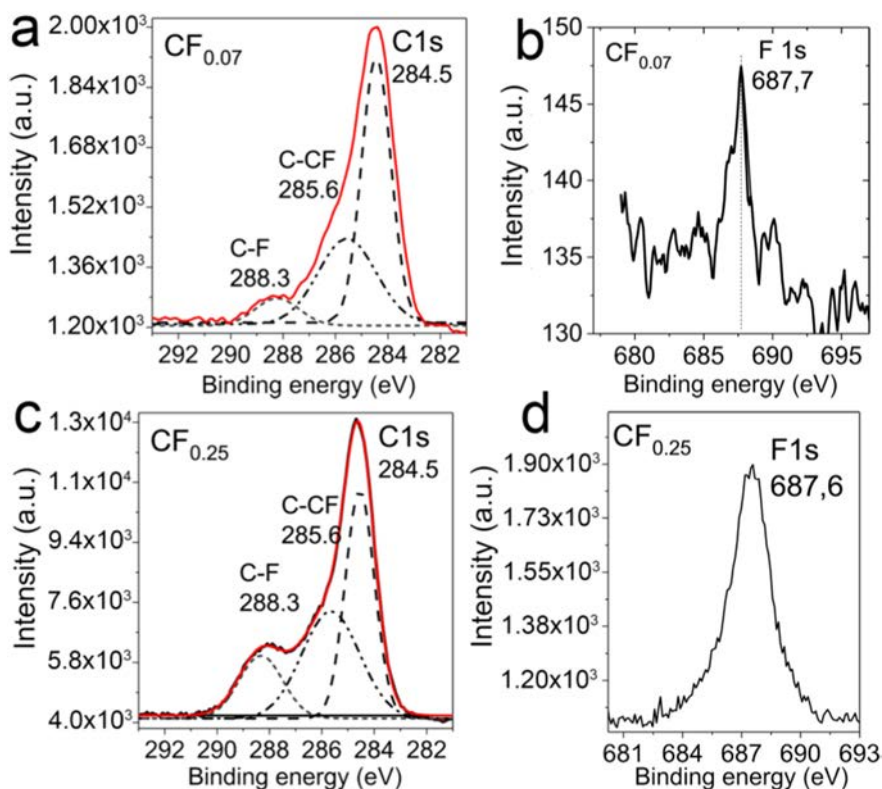


**Fig. 3.** XPS C1s (a, c) and F1s (b, d) spectra of films prepared from a non-filtered graphene suspension after two different fluorination times. The calculated fluorination degree is 7 (a, b) and 21% (c, d) (suspension A) are given in figure as parameter.

was applied onto a layer printed from Ag particles (Fig. 4(b)), in the Raman measurements a phenomenon of giant amplification of signal was observed. As a result, in the Raman spectra, apart from the features due to Ag (1160–1350 and 1480–1520  $\text{cm}^{-1}$ ), there emerged a G peak (1565  $\text{cm}^{-1}$ ) and no D peak. The appearance of the G peak in the absence of the D peak could be due to the fluorination of defects first [37,38]. Due to fluorination and formation of a band gap, some areas around defects, in time, are excluded from consideration in Raman measurements. But some non-fluorinated areas, chains still exist [27–29]. Namely, this part of the layer is observed in the giant amplification regime of the Raman signal. The broad overlapping bands with maxima at 1165–1355 and 1520  $\text{cm}^{-1}$  observed, according to [39], in the spectra of Ag nanoparticles were presumably due to Ag atoms bonded to oxygen and carbon. On the whole, the Raman spectra registered in the present study for Ag nanoparticles were similar to the data by Strelchuk [39].

HRTEM images of thin layers obtained on the application of fluorinated suspensions onto standard carbon films for HRTEM studies are shown in Fig. 5. Evidently, these layers contain ultra-dispersed crystalline particles whose sizes depend on fluorination conditions; for fluorination degrees 17 and 25%, these sizes amount respectively to 2–4 nm and 5–8 nm. For the WFG fluorination degree of 17%, the diffraction fringes are smeared, and some reflections are not observed due to the small sizes of the non-fluorinated regions in the particles. Indicative of the presence of multigraphene nanocrystals (quantum dots) in WFG is also the electronic properties of such quantum dots, which were studied in Ref. [18], where the size quantization levels of such nanocrystals were measured. The electron microdiffraction patterns for both cases are shown in the insets to Fig. 5(a) and 5(b). In the case of a high fluorination degree (25%), individual reflections located around concentric circumferences were measured. In both cases, the diffraction maxima

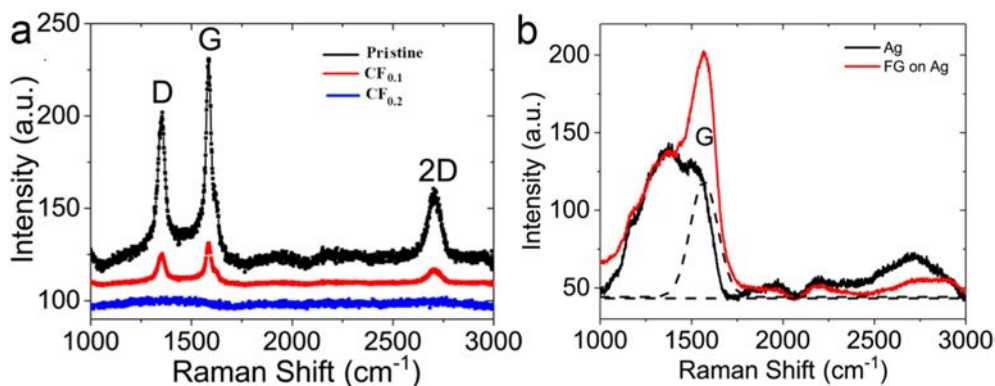


**Fig. 4.** (a) Raman spectra of films of different fluorination degrees (given as a parameter in the figure) measured on  $\text{SiO}_2/\text{Si}$  substrates. (b) Raman spectra for a fluorinated graphene layer about 10 nm thick on a contact line printed from Ag particles. The G peak was obtained by subtracting the spectrum due to Ag particles from the spectrum of the FG film on the line of Ag particles.

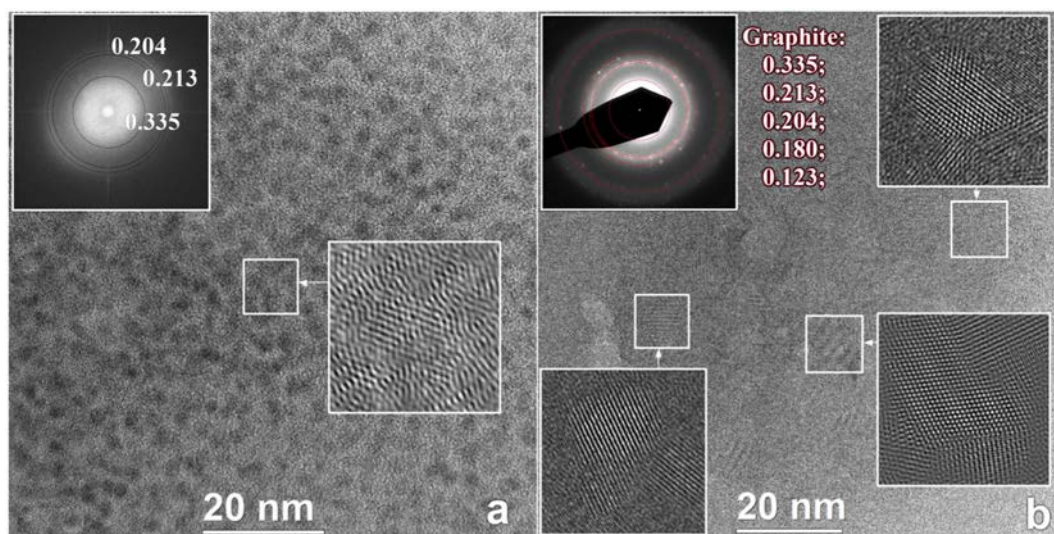


**Fig. 5.** HRTEM images of films prepared from graphene suspensions of different fluorination degrees. (a) F/C ~ 17%, (b) F/C ~ 25%. At the upper left corners of the images, electron microdiffraction patterns are shown. The white and red circles in inserts of (a, b) indicate the calculated position of reflections from the planes (002) for polycrystalline graphite (0.336, 0.213, 0.204, 0.18, 0.123). Enlarged fragments of individual nanocrystals are shown in the insets marked with white squares.

were located approximately along diffraction circumferences due to FG crystals (black and red circumferences in the insets). Those circumferences are plotted for the (002), (100), (101), (102), and (110) graphene planes (0.336, 0.213, 0.204, 0.180, and 0.123 nm, correspondingly). The interplanar-spacing values for those crystal planes are indicated in the insets to Fig. 5(a) and (b). It should be noted here that the (002) FG reference planes stretch vertically.

As it was noted above, the diffraction maxima are located approximately along the circumferences corresponding to the diffraction of multigraphene crystals. Simultaneously, it is distinctly seen that, especially for films with the fluorination degree 25%, individual diffraction reflections are located not on the circumferences marked with red color in Fig. 5(b) but closer to the center of the diffraction pattern. The latter indicates that the interplanar-spacing values in particles with fluorination degree 25% are larger than those in multigraphene. A detailed analysis of this effect was performed using a digital treatment of experimental HRTEM images by the geometrical-phase method. The geometrical phase analysis (GPA) for the first time proposed in Ref. [40] and generalized later in Ref. [41] allows one to create maps of lattice parameters over the HRTEM image area and accurately measure the lattice parameter value at each point of the image. In the present study, this method was used to analyze changes in (002) interplanar-spacing values (002) in particles that were contained in layers with fluorination degree 25%. Fig. 6(a) shows, first, HRTEM images of such particles (these particles are indicated with white circumferences) and, second, the corresponding Fourier spectrum (inset to Fig. 6a). Fig. 5(b) shows dark-field images of these particles obtained in (002)-type reflections denoted in the Fourier spectrum by digits 1 to 3. Fig. 6(c–e) shows the distributions, or maps, of (002) interplanar-spacing values over the area of the particles and the related profiles of (002) interplanar-spacing values recorded in the directions indicated with white arrows. Evidently, on moving from the center of a particle to its edges the interplanar spacing increases by 1–2%. The noticeable difference in the local interplanar distance values for the considered particles is connected with the local variation of fluorination degree. These values agree with the magnitude of the shift of reflections towards the center of diffraction pattern relative to the red ring due to polycrystalline graphite (see the inset to Fig. 6(b)). Thus, it can be concluded that the observed nanocrystals were multi-layer fluorinated graphene ones with basic planes oriented normally to the substrates. The interlayer spacing for the graphite fluorite is equal to 0.585 nm or higher

dependently on F content [42]. Fluoride atom intercalation leads to a strong increase in the interlayer spacing. In our case, as it follows from XPS data there are no intercalated fluorine atoms. The relatively weak increase in the interplanar-spacing values in flakes is most likely connected with the preferential fluorination of the atoms located at the flake surface. The decrease in the interplanar-spacing in the flake center also shows that the reaction with the fluorine prevails at the flake edges.

The transmission of FG layers of high fluorination degree (~30%) on PET substrates is shown in Fig. 7. At a film thickness of 20 nm, the transmission of FG layers is 96–98% in the visible and near IR spectral regions. In the far IR range (Fig. 7b), the absorption is also primarily defined by the substrate whereas the FG film proper induces no bands or any notable change of the absorption level in the spectra. The insets in Fig. 7(a, b) demonstrate the absorption in the PET substrate.

### 3.3. Flexibility of heterostructures with FG layers

On a PET substrate, cross-bar structures formed by intersecting contact lines were printed out from Ag particles. The particles were separated from one another by a FG film of thickness 15–40 nm (10, 20, and 30 printing pass made). Optical and SEM images of the printed Ag/FG/Ag structures and their schematics are shown in Figs. 8 and S1. In Fig. S1, Supplementary information, one can see the edge of an FG film (indicated with the arrow). The leakage current through the FG layer versus the number of printed layers and the current-voltage characteristic for a structure with 10 printed layers are shown in Fig. 8 (b) and (d). On the whole, as a summary to measurements that were performed on that structure, we conclude that, for all the three types of printed structures, the leakage currents were  $<10^{-7}$  A/cm<sup>2</sup>, and the breakdown field was  $>10^7$  V/cm. Current measurements of in the vertical configuration in crossbar structures with printed fluorinated graphene layers under the stretching strain with the bending radius of 2 mm have shown that the leakage currents were not increasing, but the current noises became more pronounced. At a PET substrate thickness of 200 nm, the magnitude of the stretching strain arising under such bending was 5%.

A wonderful combination of fluorinated graphene properties such as its ultra-small charge (see Fig. S2 in Section “Supplementary information” and in Refs. [27, 28]), ultra-low leakage currents, and the high breakdown field, and high transparency makes fluorinated graphene

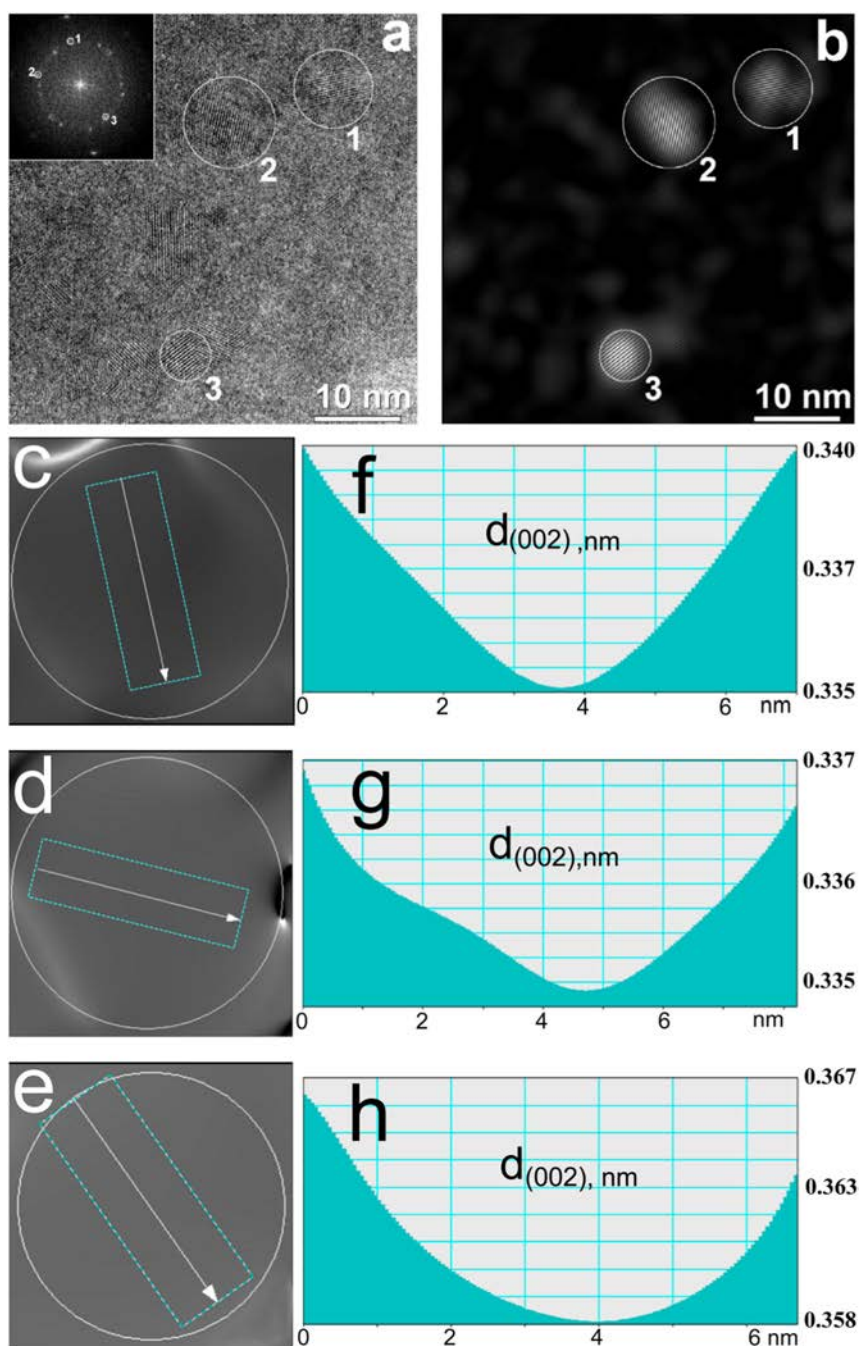


**Fig. 6.** (a) – HREM image of particles extracted from a graphene suspension with fluorination degree ~25% and the corresponding Fourier spectrum (inset); (b) – dark-field images of particles in (002)-type reflections denoted in the Fourier spectrum with digits 1–3; (c–e) – maps of (002) interplanar-spacing values on the particles areas denoted with digits 1–3 and (f–h) the respective distributions of the local interplanar-spacing values measured in the directions indicated with the white arrows.

films highly promising ones for application as carrier layers for graphene sheets (interface engineering), as a gate insulator in FET structures, etc. Presently, there are no analogs to such films.

Fig. 9 demonstrates images of a series of structures prepared on flexible PI and PET substrates and on paper. On the above substrates, structures containing Ag contacts in the form of two interpenetrating combs (Fig. 9(a)) with 3–4 interdigital fingers were printed. Such initial structures without a fluorinated graphene film were used as reference structures in bending measurements. Then, fluorinated graphene suspensions of various fluorination degrees (FG suspension with insulating properties and WFG whose film exhibited some electrical conduction) were applied onto the structures. Depending on the type of the applied suspension, FG or WFG, the capacitance values of the structure at three

frequencies of the ac signal, 1 MHz, 100 kHz, and 10 kHz, and the conductivity of the structure, or its current-voltage characteristic, were measured. An optical image of the structure on a polyimide film taken during measurements is shown in Fig. 9(b). The parameters of the structures are indicated in Fig. S3, Supplementary information. Measurements were additionally carried out for the position of the structure turned through an angle of 90° with respect to its position in Fig. 9 (b) (see insert in Fig. S4(a)), where the contact pads to accept the probes were located across the bending axis of the structure. It turned out that the rotation of the structures with 3–4 interdigital fingers (90°) exerted no substantial influence on the measured characteristics. The film thickness  $t$  versus the number of deposited layers varied in the interval from 10 to 50 nm. Fig. 9(c) shows the thickest (50 nm) film at

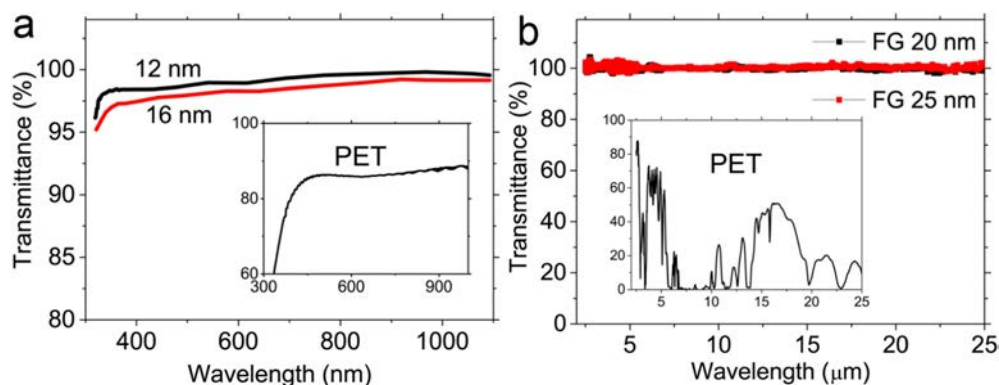
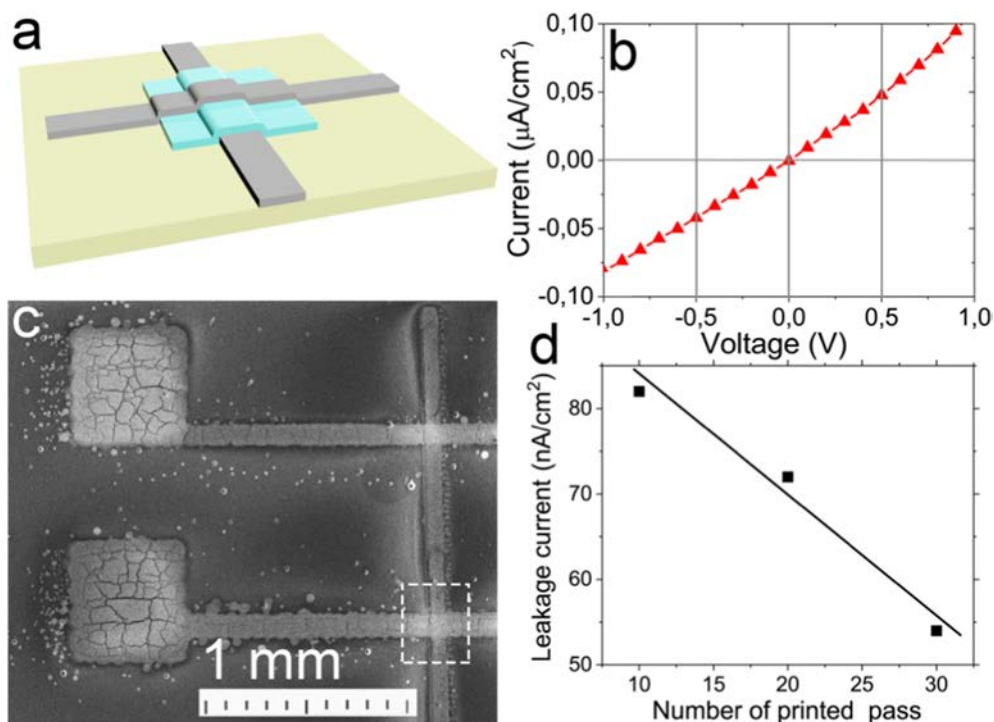


**Fig. 7.** Light transmission through thin FG films on a PET substrate in different wavelength ranges. (a) Transmission in the visible and near-IR spectral region measured in differential mode with the subtraction of the transmission of a structure with an FG film from that of PET installed in the reference channel. The thickness of the FG film is indicated by the digits at the curves. (b) Transmission in the far-IR spectral region. At the curves, the thickness of the fluorinated graphene films is indicated. Transmission through the PET substrate in different wavelength ranges is shown in the insets.

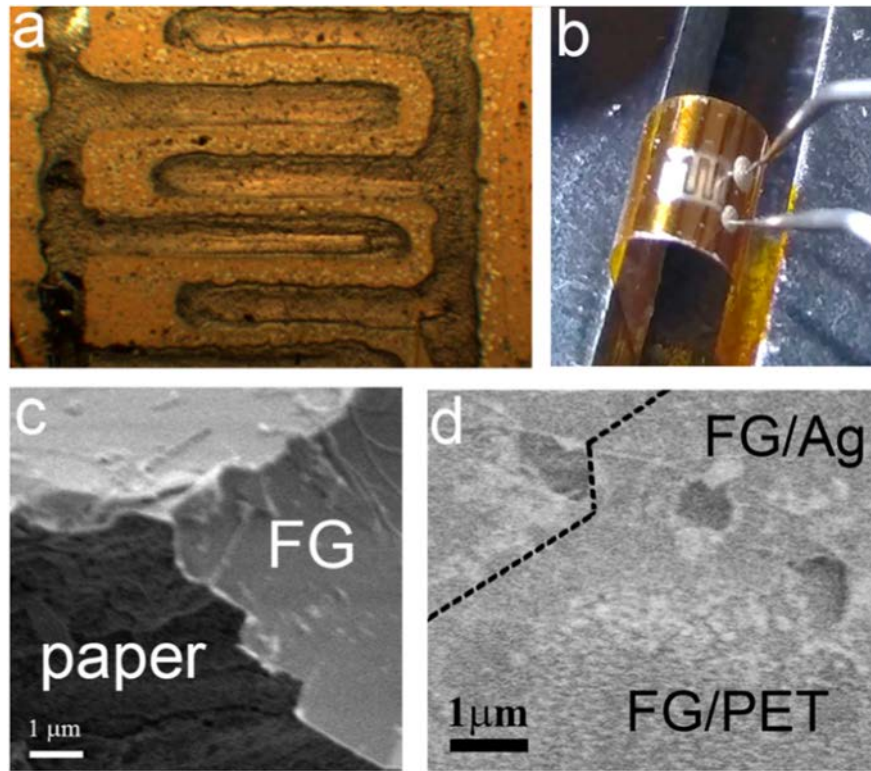
the edge of the paper substrate, and Fig. 9(d), a WFG film going from Ag contacts to the PET film.

Fig. 10 shows the capacitance and resistance of the structures on the bending radius of the substrate for the insulating-FG-film structure. It is seen that the capacitance of the reference structure without an FG film remained almost unchanged in the studied range of bending radii and strains. On the opposite, the capacitance of a structure with an FG film somewhat decreased at bending radii  $< 2$  mm. The mechanical strain  $\varepsilon$  that had arisen in the film was estimated (see, e.g. [43]) from the expression  $\varepsilon = (d + t)/2r$ , where  $d$  is the thickness of the flexible substrate (here, the film thickness of 10–50 nm could be neglected in comparison with the substrate), and  $r$  is the substrate bending radius. The magnitude of the changes of capacitance proved to be 3–4% for stretching strains  $\varepsilon$  of 2.5%. The leakage currents across the studied films were the order of several picoamperes at  $10^{-3}$  cm<sup>2</sup> contact area (current density  $\sim 10^{-8}$  A/cm<sup>2</sup>), and it did not increase on bending. Current-voltage characteristics of the structures with WFG films

measured at different bending radii proved to be linear. Fig. S4 (a) shows current-voltage characteristics of one of the structures at different bending radii. From these characteristics, the resistance  $R$  of the structure was calculated to obtain the dependence of the resistance on the substrate bending radius (Fig. 10(b)). Notable changes in resistance were observed at bending radii  $< 2.5$  mm (strains  $> 4\%$ ). Repeated measurements of the current in one of the structures have shown (see also Fig. S4(b) in Supplementary information) the presence of data scatter both in the initial resistance of the structures and in the resistance value at bending radii of 1 mm. The value of resistance changes  $\Delta R/R_0$  proved to be in the range of 14–28% with a different sign at 10% stretching strains (bending radius 1 mm). The scattering of the initial resistance values at large bending radii or without bending is most likely connected with a high resistivity of fluorinated films found to be within  $\pm 15\%$ . Besides, a comparison of the resistance values before and after the measurement cycle showed that the resistance of the structure was almost not different from the initial value. Multiple bendings up



**Fig. 8.** (a) Schematic and (c) SEM image of printed crossbar Ag/FG/Ag structures. The dashed rectangle in the optical image shows the size and location of the printed fluorinated graphene layer. (b) Current-voltage characteristic for ten printed FG layers. (d) The leakage current through the FG layer as a function of the printed layer number at a bias voltage of 1 V.



**Fig. 9.** Optical and SEM images of structures created by the application of FG onto flexible substrates with printed Ag contacts: structures on (a, b) polyimide (PI) films, (c) paper, and (d) polyethyleneterephthalate (PET).

to 10% strain did not result in the breakage of the film, and they did not cause notable changes in their properties after several tens of deformation cycles. The results of cycling at the strain value of  $\pm 0.15\%$  given in Fig. S5 in Supporting information show that there is no degradation of the film properties under the action of the cycles of relatively weak tensile or compressive strains. It is important to mention here that the film consists of a large number of flakes, basal planes of flakes are located not only horizontally on the substrate. Part of the flakes is located at different angles. As a result of film bending, the flakes are subjected to different deformation types (symmetrical and asymmetrical stretching, shear and non-uniform deformations). The resulting bending effects on such mesoscopic system are found can vary under repeated measurements.

Even a small change in the fixation of the tested structure in a holder results in a new reaction on the bending.

Also, we performed measurements of the changes in resistance for an Ag line printed on a 50- $\mu\text{m}$  thick polyimide film and on the 200- $\mu\text{m}$  thick PET. It was shown (see Fig. S6 in Supplementary information) that on bending deformations with bending radius 1 mm the resistance of the printed lines remained unchanged. For 50- and 200- $\mu\text{m}$  thick films and 1-mm bending radius the magnitude  $\epsilon$  of the stretching strains was 2.5 and 10%, respectively.

Fluorographene is known to have a relatively low Young's modulus of  $E = 100 \pm 30 \text{ N/m}$ , and intrinsic strength  $\sigma = 15 \text{ N/m}$  [7]. For comparison, for graphene we have  $E = 340 \pm 50 \text{ N/m}$  and  $\sigma = 42 \pm 4 \text{ N/m}$ ,

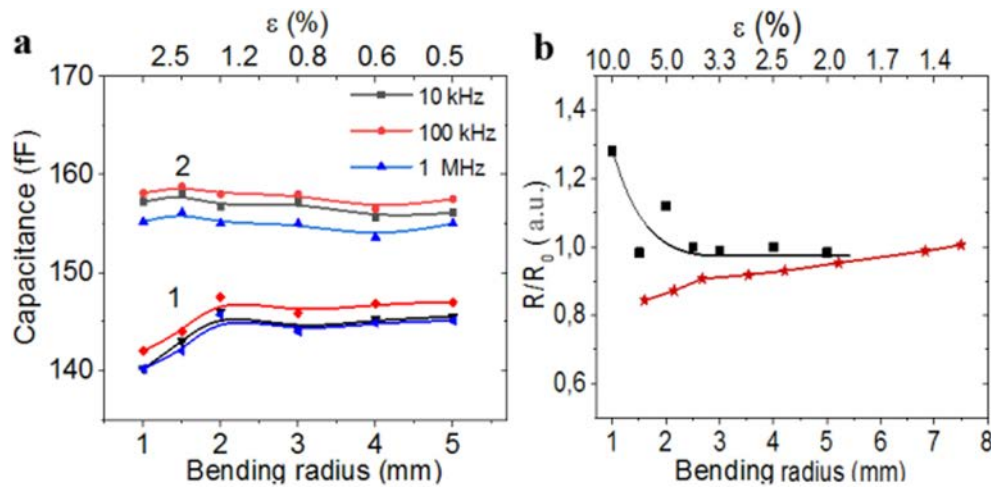


**Fig. 10.** (a) The capacitance of structures obtained on PI (thickness 50  $\mu\text{m}$ ) with printed Ag contacts versus the bending radius of the structures: 1 – Structures with an applied FG film; 2 – the initial structure without an FG film. The capacitance was measured at three frequencies, 1 MHz, 100 kHz, and 10 kHz (FG permittivity is 1.2). (b) The relative resistance of a WFG-on-PET structure (substrate thickness 200  $\mu\text{m}$ ) versus the bending radius and strain value (two repeated measurements).

respectively. It should be noted here that the values of those parameters are rather high in comparison with many other materials. Moreover, the ratio  $\sigma/E$  yields value of 0.12 and 0.15, and both materials can be expected capable of withstanding strains amounting to 12–15%. The only experiments on studying the mechanical properties of fluorographene were performed by Nair [7], in this study, deformations at which the rupture of graphene and fluorographene membranes acted upon by an AFM probe occurred were measured; the found values proved to be nearly identical. In our case, when the fluorinated graphene films were created from a suspension, the film properties can be different from that expected for fluorographene. The variation of the resistance changes under the strain in repeated measurements is most likely connected with non-uniform deformations of different types arising in the film formed from flakes. As it is summarized in the review [44], different types of deformations lead to various effects (not only an increase and decrease of the resistance [45]) but also a change of the electronic structure and appearance of the band gaps in some flakes [46,47]. The shear deformation has to lead to more significant effects than the bending one [48]. The non-uniform shear deformation in combination with the bending for the mesoscopic system causes a variation in resistivity under repeated measurements. The obtained data allow us to state that the strain related effect on the film resistance is not very pronounced against the background of the resistance spreading. Generally, the observed weak changes in the capacity of insulating layers and resistivity of conducting films under bending allow us to tell about the perspectives of fluorinated graphene films created from suspension for flexible electronics.

On the whole, measurements performed on structures with a fluorinated graphene film demonstrate a high potential of the films when used in heterostructures for flexible electronics [48]. On making a comparison with graphene properties [44], fluorinated graphene comes as a good counterpart for graphene. For comparison, we can cite data for other dielectrics which were used as gate dielectrics in graphene-channel FET structures on flexible substrates. For  $\text{Al}_2\text{O}_3$ , 8.7-% changes of FET characteristics were observed at 4.6-% stretching strain [49–52]. For  $\text{HfO}_2$ , the characteristics remained unchanged up to strains of 1.75% [53]. In the case in which h-BN was used, FETs became unserviceable at about 1-% strains [54]. Moreover, it has been recently demonstrated that the mechanical properties of h-BN, practically, do not change with a decrease in flake thickness [55]. In the case of printed FET with the use of gate from h-BN suspension, the strong change in FET characteristics at bending is demonstrated [6]. FET-like structures with a graphene channel were created with the bottom FG gate and a strong increase in electron mobility in the graphene channel, and conductivity of the FG capsulated graphene film were found [21]. Thus, the obtained stability of fluorinated graphene characteristics looks promising for its use in flexible electronics. It should be noted here that the degree of fluorination of isolating FG films is normally not high, 30–40%, and this factor can appear a determining one for the comparable mechanical properties of graphene and fluorinated graphene. Similarly, numerous studies of graphene oxide flexibility (typical oxidation degree ~ 40%) have also demonstrated nearly identical mechanical properties of graphene and graphene oxide [56,57].

#### 4. Conclusions

Structural, electrical, and optical properties of fluorinated graphene (FG) flakes obtained by treatment of multigraphene suspension in aqueous solutions of hydrofluoric acid were studied. It was shown that the fluorination time is defined by the initial sizes of graphene particles: decreasing the sizes of initial graphene flakes from several micrometers to 400 nm decreases the time required for obtaining  $\text{C}_2\text{F}$  from ~40–60 to 1–2 days. Depending on fluorination time, the FG flakes become smaller with sizes ranged from 3 to 10 nm to micrometers. Using the HRTEM method, it was established that at fluorination degree >23% a smooth increase of (002) interplanar spacing by 1–2% from the

center of fluorinated nanocrystals to their edges was observed. At fluorination degree <23%, few-layer graphene nanocrystals sized 4–7 nm were observed in the fluorinated graphene matrix. For the used fluorination procedure, the XPS spectra of the FG film exhibited only peaks C—C (284.5 eV), C—CF (285.6 eV), and CF (288.3 eV) bonds, and no indications for  $\text{CF}_x$  bonds with  $x > 1$  were observed. After fluorination only in the regime of giant amplification of Raman scattering the G peak ( $1590\text{ cm}^{-1}$ , C—C bonds) was observed in spectra with simultaneous absence of the defect-related D peak. This observation proved both the absence of dangling bonds and the presence of non-fluorinated chains or regions formed by non-fluorinated carbon atoms in the core of flakes. At fluorination degree in excess of 23%, fluorinated graphene films possessed dielectric properties. The leakage currents at the thickness of FG films of 20–40 nm in the 2D printed cross-bar structures were  $<0.1\text{ }\mu\text{A}/\text{cm}^2$ , and the breakdown field was  $>5 \times 10^6\text{ V}/\text{cm}$ . Such characteristics in combination with the low level of the charge in the FG film and at its interfaces with other materials make fluorinated graphene films a promising gate material and a material for preparation of insulating layers in heterostructures involving sheets of 2D materials. A study of the properties of fluorinated graphene films applied onto printed Ag contacts under bending of the substrate (paper, polyimide films, and PET) has proven the stability of characteristics of the substrates accurate to several percents up to stretching strains of 2.5–4%. For instance, the leakage current through 50 nm of the film proved to be  $10^{-7}$ – $10^{-8}\text{ A}/\text{cm}^2$ , and they showed no increase upon bending. Multiple bendings did not result in the breakage of the film, nor did they cause notable changes in their properties after several tens of deformation cycles. The obtained results prove the high potential of fluorinated graphene films in flexible electronics.

#### Author contributions

I.V.A. and S.A.S. conceived the strategy of the study, I.I.K., A.I.I. and N.A.N. performed all electrical and bending characterizations, A.K.G. performed TEM and HREM measurements, I.A.K. fabricated all printed layers and structures, R.A.S. created fluorinated graphene suspension, I.V.A. wrote the paper and supervised the whole project.

#### Data availability

The raw/processed data required to reproduce these findings cannot be shared at this time due to technical or time limitations.

#### Acknowledgments

HRTEM studies were performed using the equipment of CCU “Nanostructures” with the support of RSF (Grant No. 14-22-00143). The participation of I.I.K. in the work was supported by a grant from the Russian Foundation for Basic Research (Grant. No 17-32-5003).

#### Appendix A. Supplementary data

Supplementary data to this article can be found online at <https://doi.org/10.1016/j.matdes.2018.11.061>.

#### References

- [1] L. Britnell, R.V. Gorbachev, R. Jalil, B.D. Belle, F. Schedin, A. Mishchenko, T. Georgiou, M.I. Katsnelson, L. Eaves, S.V. Morozov, N.M.R. Peres, J. Leist, A.K. Geim, K.S. Novoselov, L. Ponomarenko, A field-effect tunneling transistor based on vertical graphene heterostructures, *Science* 335 (2012) 947–950.
- [2] S.J. Haigh, A. Gholinia, R. Jalil, S. Romani, L. Britnell, D.C. Elias, K.S. Novoselov, L.A. Ponomarenko, A.K. Geim, R. Gorbachev, Cross-sectional imaging of individual layers and buried interfaces of graphene-based heterostructures and superlattices, *Nat. Mater.* 11 (2012) 764–767.
- [3] L. Wang, I. Meric, P.Y. Huang, Q. Gao, Y. Gao, H. Tran, T. Taniguchi, K. Watanabe, L.M. Campos, D.A. Muller, J. Guo, P. Kim, J. Hone, K.L. Shepard, C.R. Dean, One-dimensional electrical contact to a two-dimensional material, *Science* 342 (2013) 614–617.

- [4] L. Banszerus, M. Schmitz, S. Engels, J. Dauber, M. Oellers, F. Haupt, K. Watanabe, T. Taniguchi, B. Beschoten, C. Stampfer, Ultrahigh-mobility graphene devices from chemical vapor deposition on reusable copper, *Sci. Adv.* 1 (2015), 1500222.
- [5] A. Falin, Q. Cai, E.J.G. Santos, D. Scullion, D. Qian, R. Zhang, Z. Yang, S. Huang, K. Watanabe, T. Taniguchi, M.R. Barnett, Y. Chen, R.S. Ruoff, L.H. Li, Mechanical properties of atomically thin boron nitride and the role of interlayer interactions, *Nat. Commun.* 8 (2017), 15815.
- [6] T. Carey, S. Cacovich, G. Divitini, J. Ren, A. Mansouri, J.M. Kim, C. Wang, C. Ducati, R. Sordan, F. Torrisi, Fully inkjet-printed two-dimensional material field-effect heterojunctions for wearable and textile electronics, *Nat. Commun.* 8 (2017) 1202.
- [7] R.R. Nair, W.C. Ren, R. Jalil, I. Riaz, V.G. Kravets, L. Britnell, P. Blake, F. Schedin, A.S. Mayorov, S. Yuan, M.I. Katsnelson, H.M. Cheng, W. Strupinski, L.G. Bulusheva, A.V. Okotrub, I.V. Grigorieva, A.N. Grigorenko, K.S. Novoselov, A.K. Geim, Fluorographene: two dimensional counterpart of teflon, *Small* 6 (2010) 2877–2884.
- [8] J.T. Robinson, J.S. Burgess, C.E. Junkermeier, S.C. Badescu, T.L. Reinecke, F.K. Perkins, M.K. Zalalutdinov, J.W. Baldwin, J.C. Culbertson, P.E. Sheehan, E.S. Snow, Properties of fluorinated graphene films, *Nano Lett.* 10 (2010) 3001–3005.
- [9] R. Zboril, F. Karlicky, A.B. Bourlino, T.A. Steriotti, A.K. Stubos, V. Georgakilas, K. Safarova, D. Jancik, C. Trapalis, M. Otyepka, Graphene fluoride: a stable stoichiometric graphene derivative and its chemical conversion to graphene, *Small* 6 (2010) 2885–2891.
- [10] D.D. Chronopoulos, A. Bakandritsos, M. Pykal, R. Zbořil, M. Otyepka, Chemistry, properties, and applications of fluorographene, *Appl. Mat. Today* 9 (2017) 60–70.
- [11] W. Feng, P. Long, Y. Feng, Y. Li, Two-dimensional fluorinated graphene: synthesis, structures, properties and applications, *Adv. Sci.* 3 (2016), 1500413.
- [12] W.-K. Lee, J.T. Robinson, D. Gunlycke, R.R. Stine, C.R. Tamanaha, W.P. King, P.E. Sheehan, Chemically isolated graphene nanoribbons reversibly formed in fluorographene using polymer nanowire masks, *Nano Lett.* 11 (2011) 5461–5464.
- [13] R. Stine, W.-K. Lee, K.E. Whitener Jr., J.T. Robinson, P.E. Sheehan, Chemical stability of graphene fluoride produced by exposure to  $\text{XeF}_2$ , *Nano Lett.* 13 (2013) 4311–4316.
- [14] K.-I. Ho, J.-H. Liao, C.-H. Huang, C.-L. Hsu, W. Zhang, A.-Y. Lu, L.-J. Li, C.-S. Lai, C.-Y. Su, One-step formation of a single atomic-layer transistor by the selective fluorination of a graphene film, *Small* 10 (2014) 989–997.
- [15] O. Jankovsky, V. Máznek, K. Klímová, D. Sedmidubský, J. Kosina, M. Puma, Z. Sofer, Simple synthesis of fluorinated graphene: thermal exfoliation of fluorographite, *Chem. Eur. J.* 22 (2016) 17696–17703.
- [16] Z. Wang, J. Wang, Z. Li, P. Gong, X. Liu, L. Zhang, J. Ren, H. Wang, S. Yang, Synthesis of fluorinated graphene with tuneable degree of fluorination, *Carbon* 50 (2012) 5403–5410.
- [17] X. Gao, X. (Shirley) Tang, Effective reduction of graphene oxide thin films by fluorinating agent: diethylamino sulfur trifluoride, *Carbon* 76 (2014) 133–140.
- [18] K. Samanta, S. Some, Y. Kim, Y. Yoon, M. Min, S.M. Lee, Y. Park, H. Lee, Highly hydrophilic and insulating fluorinated reduced graphene oxide, *Chem. Commun.* 49 (2013) 8991–8993.
- [19] X. Zheng, M. Zhang, X. Shi, G. Wang, L. Zheng, Y. Yu, A. Huang, P.K. Chu, H. Gao, W. Ren, Z. Di, X. Wang, Fluorinated graphene in interface engineering of Ge-based nanoelectronics, *Adv. Funct. Mater.* 25 (2015) 1805–1813.
- [20] M. Zhu, X. Xie, Y. Guo, P. Chen, X. Ou, G. Yu, M. Liu, Fluorographene nanosheets with broad solvent dispersibility and their applications as a modified layer in organic field-effect transistors, *Phys. Chem. Chem. Phys.* 15 (2013) 20992–21000.
- [21] I.V. Antonova, I.A. Kotin, I.I. Kurkina, A.I. Ivanov, E.A. Yakimchuk, N.A. Nebogatikova, V.I. Vdovin, A.K. Gutakovskii, R.A. Soots, Graphene/fluorinated graphene systems for a wide spectrum of electronics application, *J. Material Science & Eng.* 6 (2017) 1000379.
- [22] I. Jeon, M.J. Ju, J. Xu, H. Choi, J. Seo, M. Kim, I.T. Choi, H.M. Kim, J.C. Kim, J. Lee, H.K. Liu, H.K. Kim, S. Dou, L. Dai, J. Baek, Edge-fluorinated graphene nanoplatelets as high performance electrodes for dye-sensitized solar cells and lithium ion batteries, *Adv. Funct. Mater.* 25 (2015) 1170–1179.
- [23] L. Zhan, S. Yang, Y. Wang, Y. Wang, L. Ling, X. Feng, Fabrication of fully fluorinated graphene nanosheets towards high-performance lithium storage, *Adv. Mat. Interf.* 1 (2014), 1300149.
- [24] J. Xie, C. Li, Z. Cui, X. Guo, Transition-metal-free magnesium-based batteries activated by anionic insertion into fluorinated graphene nanosheets, *Adv. Funct. Mater.* 25 (2015) 6519–6526.
- [25] M. Dubecský, E. Otyepková, P. Lazar, F. Karlický, M. Petr, K. Čépe, P. Banáš, R. Zbořil, M. Otyepka, Reactivity of fluorographene: a facile way toward graphene derivatives, *J. Phys. Chem. Lett.* 6 (2015) 1430–1434.
- [26] N.A. Nebogatikova, I.V. Antonova, V.Ya. Prinz, Functionalization of graphene and few-layer graphene with aqueous solution of hydrofluoric acid, *Phys. E* 52 (2013) 106–111.
- [27] N.A. Nebogatikova, I.V. Antonova, V.Ya. Prinz, V.B. Timofeev, S.A. Smagulova, Graphene quantum dots in fluorographene matrix formed by means of chemical functionalization, *Carbon* 77 (2014) 1095–1103.
- [28] N.A. Nebogatikova, I.V. Antonova, V. Ya. I.I. Prinz, G.N. Kurkina, V.B. Aleksandrov, S.A. Timofeev, E.R. Smagulova, V.G. Kesler Zakirov, Fluorinated graphene dielectric films obtained from functionalized graphene suspension: preparation and properties, *Phys. Chem. Chem. Phys.* 17 (2015) 13257–13266.
- [29] I.V. Antonova, N.A. Nebogatikova, V. Ya. Prinz, Self-organized arrays of graphene and few-layer graphene quantum dots in fluorographene matrix: formation of quantum dots and charge spectroscopy, *Appl. Phys. Lett.* 104 (2014), 193108.
- [30] I.V. Antonova, I.I. Kurkina, N.A. Nebogatikova, A.I. Komonov, S.A. Smagulova, Films fabricated from partially fluorinated graphene suspension: structural, electronic properties and negative differential resistance, *Nanotechnology* 28 (2017), 074001.
- [31] F.D. Vasilieva, A.N. Kapitonov, E.A. Yakimchuk, I.A. Kotin, S.A. Smagulova, I.V. Antonova, Mildly oxidized graphene oxide suspension for printed technologies, *Mater. Res. Express* 5 (2018), 065608.
- [32] P. Gong, Z. Wang, Z. Li, Y. Mi, J. Sun, L. Niu, H. Wang, J. Wang, S. Yang, Photochemical synthesis of fluorinated graphene via a simultaneous fluorination and reduction route, *RSC Adv.* 3 (2013) 6327–6330.
- [33] R.B. dos Santos, R. Rivelino, F. de B. Mota, G.K. Gueorguiev, Exploring hydrogenation and fluorination in curved 2D carbon systems: a density functional theory study on corannulene, *J. Phys. Chem. A* 116 (2012) 9080–9087.
- [34] Y. Wang, W.C. Lee, K.K. Manga, P.K. Ang, J. Lu, Y.P. Liu, C.T. Lim, K.P. Loh, Fluorinated graphene for promoting neuro-induction of stem cells, *Adv. Mater.* 24 (2012) 4285–4331.
- [35] X. Wang, Y. Dai, J. Gao, J. Huang, B. Li, C. Fan, J. Yang, X. Liu, High-yield production of highly fluorinated graphene by direct heating fluorination of graphene-oxide, *ACS Appl. Mater. Interfaces* 5 (2013) 8294–8299.
- [36] Y. Xu, A. Ali, K. Shehzad, N. Meng, M. Xu, Y. Zhang, X. Wang, C. Jin, H. Wang, Y. Guo, Z. Yang, B. Yu, Y. Liu, Q. He, X. Duan, X. Wang, P.-H. Tan, W. Hu, H. Lu, T. Hasan, Solvent-based soft-patterning of graphene lateral heterostructures for broadband high-speed metal–semiconductor–metal photodetectors, *Adv. Mater. Technol.* 2 (2017), 1600241.
- [37] A.C. Ferrari, J. Robertson, Interpretation of Raman spectra of disordered and amorphous carbon, *Phys. Rev. B* 61 (2000) 14095–14107.
- [38] S. Ryu, J. Maultzsch, M.Y. Han, P. Kim, L.E. Brus, Raman spectroscopy of lithographically patterned graphene nanoribbons, *ACS Nano* 5 (2011) 4123–4130.
- [39] V.V. Strelchuk, O.F. Kolomy, B.O. Golichenko, M.I. Boyko, E.B. Kaganovich, I.M. Krishchenko, S.O. Kravchenko, O.S. Lytvyn, E.G. Manoilov, I.M. Nasieka, Micro-Raman study of nanocomposite porous films with silver nanoparticles prepared using pulsed laser deposition, *Semicond. Phys. Quant. Elect. & Optoelect.* 18 (2015) 46–52.
- [40] M.J. Hÿtch, E. Snoeck, R. Kilaas, Quantitative measurement of displacement and strain fields from HREM micrographs, *Ultramicroscopy* 74 (1998) 131–146.
- [41] A.K. Gutakovskii, A.L. Chuvilin, S.A. Song, Application of high-resolution electron microscopy for visualization and quantitative analysis of strain fields in heterostructures, *Bull. Russian Acad. Sci.: Phys.* 71 (2007) 1426–1430.
- [42] D. Song, A. Mahajan, E.B. Secor, M.C. Hersam, L.F. Francis, C.D. Frisbie, High-resolution transfer printing of graphene lines for fully printed, flexible electronics, *ACS Nano* 11 (2017) 7431–7439.
- [43] N. Watanabe, T. Nakajima, H. Touhara, Studies in inorganic chemistry, Graphite Fluorides, vol. 8, Elsevier, Amsterdam, 1988.
- [44] J. Zhao, G.-Y. Zhang, D.-X. Shi, Review of graphene-based strain sensors, *Chin Phys B* 22 (2013), 057701.
- [45] K.S. Kim, Y. Zhao, H. Jang, S.Y. Lee, J.M. Kim, K.S. Kim, J.-H. Ahn, P. Kim, J.-Y. Choi, B.H. Hong, Large-scale pattern growth of graphene films for stretchable transparent electrodes, *Nature* 457 (2009) 706–710.
- [46] G. Cocco, E. Cadelano, L. Colombo, Gap opening in graphene by shear strain, *Phys. Rev. B* 81 (2010), 241412.
- [47] S.-M. Choi, S.-H. Jhi, Y.-W. Son, Effects of strain on electronic properties of graphene, *Phys. Rev. B* 81 (2010) 081407.
- [48] I.V. Antonova, Non-organic dielectric layers for graphene and flexible electronics, *Int. J. Nanomater. Nanotechnol. Nanomed.* 2 (2016) 0.18–0.24.
- [49] J. Lee, L. Tao, Y. Hao, R.S. Ruoff, D. Akinwande, Embedded-gate graphene transistors for high-mobility detachable flexible nanoelectronics, *Appl. Phys. Lett.* 100 (2012), 152104.
- [50] S. Lee, O.D. Iyore, S. Park, Y.G. Lee, S. Jandhyala, C.G. Kang, G. Mordiy, Y. Kim, M. Quainedo-Lopez, B.E. Gnade, R.M. Wallace, B.H. Lee, J. Kim, Rigid substrate process to achieve high mobility in graphene field-effect transistors on a flexible substrate, *Carbon* 68 (2014) 791–797.
- [51] J. Lee, L. Tao, K.N. Parrish, Y. Hao, R.S. Ruoff, D. Akinwande, Multi-finger flexible graphene field-effect transistors with high bendability, *Appl. Phys. Lett.* 101 (2012), 252109.
- [52] N. Petrone, I. Meric, J. Hone, K.L. Shepard, Graphene field-effect transistors with gigahertz-frequency power gain on flexible substrates, *Nano Lett.* 13 (2013) 121–125.
- [53] N. Petrone, T. Chari, I. Meric, L. Wang, K.L. Shepard, J. Home, Flexible graphene field-effect transistors encapsulated in hexagonal boron nitride, *ACS Nano* 9 (2015) 8953–8959.
- [54] H.J. Park, W.-J. Kim, H.-K. Lee, D.-S. Lee, J.-H. Shin, Y. Jun, Y.J. Yun, Highly flexible, mechanically stable, and sensitive  $\text{NO}_2$  gas sensors based on reduced graphene oxide nanofibrous mesh fabric for flexible electronics, *Sensors Actuators B* 257 (2018) 846–852.
- [55] A. Falin, Q. Cai, E.J.G. Santos, D. Scullion, D. Qian, R. Zhang, Z. Yang, S. Huang, K. Watanabe, T. Taniguchi, M.R. Barnett, Y. Chen, R.S. Ruoff, L.H. Li, Mechanical properties of atomically thin boron nitride and the role of interlayer interactions, *Nat. Com.* 6 (2017) 15815.
- [56] C. Ogata, R. Kurogi, K. Awaya, K. Hatakeyama, T. Taniguchi, M. Koinuma, Y. Matsumoto, All-graphene oxide flexible solid-state supercapacitors with enhanced electrochemical performance, *ACS Appl. Mater. Interf.* 9 (2017) 26151–26160.
- [57] W.-S. Jiang, Z.-B. Liu, W. Xin, X.-D. Chen, J.-G. Tian, Reduced graphene oxide nanosheets for flexible and stretchable conductors, *Nanotechnology* 27 (2016), 09530.